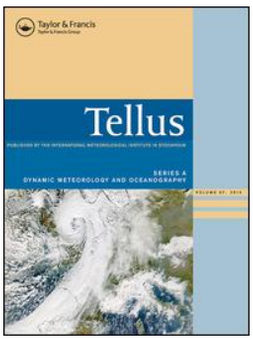

Tellus A: Dynamic Meteorology and Oceanography

ISSN: (Print) 1600-0870 (Online) Journal homepage: http://www.tandfonline.com/loi/zela20

Asymmetric response of the Atlantic Meridional Ocean Circulation to freshwater anomalies in a strongly-eddying global ocean model

Sandra-Esther Brunnabend & Henk A. Dijkstra

To cite this article: Sandra-Esther Brunnabend & Henk A. Dijkstra (2017) Asymmetric response of the Atlantic Meridional Ocean Circulation to freshwater anomalies in a strongly-eddying global ocean model, Tellus A: Dynamic Meteorology and Oceanography, 69:1, 1299283, DOI: 10.1080/16000870.2017.1299283

To link to this article: https://doi.org/10.1080/16000870.2017.1299283

Published online: 03 Apr 2017.

Tellus
SERIES A
DYANAMIC
METEOROLOGY
AND OCEANOGRAPHY
PUBLISHED BY THE INTERNATIONAL METEOROLOGICAL INSTITUTE IN STOCKHOLM

Asymmetric response of the Atlantic Meridional Ocean Circulation to freshwater anomalies in a strongly-eddying global ocean model

By SANDRA-ESTHER BRUNNABEND[1,2] and HENK A. DIJKSTRA[1]*, [1]*Institute for Marine and Atmospheric Research Utrecht, Department of Physics and Astronomy, Utrecht University, Utrecht, The Netherlands;* [2]*Leibniz Institute for Baltic Sea Research Warnemünde, Rostock, Germany*

(Manuscript received 22 December 2016; in final form 23 January 2017)

ABSTRACT

The Atlantic Meridional Overturning Circulation (AMOC) responds sensitively to density changes in regions of deepwater formation. In this paper, we investigate the nonlinear response of the AMOC to large amplitude freshwater changes around Greenland using a strongly-eddying global ocean model. Due to a 0.5 Sv freshwater input, the maximum AMOC at 35°N decreases by about 50% over a 45 year period. The AMOC does not recover over a period of 50 years when the freshwater input is ceased at year 45. However, when reversing the sign of the freshwater input at year 45, the AMOC needs only about 10 years to fully recover. The mechanism that causes this asymmetric response in the AMOC is clarified using water mass transformation theory.

Keywords: AMOC, high-resolution ocean modeling, hosing, Parallel Ocean Program

1. Introduction

The Atlantic Meridional Overturning Circulation (AMOC) is that part of the Atlantic Ocean circulation that is mainly responsible for the meridional transport of heat and salt in the Atlantic Ocean (Johns et al., 2011). It is thought to be sensitive to freshwater anomalies in the northern North Atlantic affecting the sinking and redistribution of water masses. Such a sensitivity is found in a hierarchy of climate models, ranging from ocean-box models (Stommel, 1961) to global climate (CMIP5) models (Drijfhout et al., 2015). A mechanism that is causing this sensitivity is the so-called salt advection feedback. A freshwater perturbation in the northern Atlantic leads to a weakening of the AMOC, which in turn leads to a reduction in meridional salt transport, hence amplifying the original perturbation (Stommel, 1961; Wolfe and Cessi, 2014).

There are many global ocean-climate model studies that discuss the sensitivity of the AMOC to freshwater perturbations. One of the typical simulations carried out with these models focusses on the AMOC response to freshwater anomalies associated with Greenland Ice Sheet melting (Gerdes et al., 2006; Stammer, 2008; Kopp et al., 2010; Stammer et al., 2011). These models mostly employ a freshwater inflow of 0.1 Sv (1 Sv $= 1 \times 10^6$ m^3 s^{-1}) and a horizontal resolution of about 1.0° such that the effects of ocean eddies are parameterized. In these non-eddying ocean/climate models, the AMOC is weakening in response to the freshwater input, but there is quite some variation between models. In a relative short simulation (10 years) with an eddy-permitting (ORCA025) model (Marsh et al., 2010) the freshwater anomalies remain localized to the area of the Labrador Sea and hence (on this short time scale) the impact on the large-scale circulation is limited. Behrens et al. (2013) showed that ocean-only models with an eddy-permitting (0.25°) resolution are quite sensitive with respect to the surface boundary condition formulation used.

Weijer et al. (2012) used the Parallel Ocean Program (POP) in two configurations, with horizontal resolutions of 1° and 0.1°, respectively. The transient AMOC response to the addition of 0.1 Sv of freshwater was significantly different between the two configurations (Weijer et al., 2012). In the low-resolution version of the model, the AMOC strength levels off after a rapid initial decline, while in the high-resolution configuration, the AMOC decline is more gradual and persistent. In addition, only in the high-resolution configuration the oceanic response is found to be strongly dependent on where the anomalous freshwater forcing is applied. Using the same configuration as in Weijer et al. (2012),

*Corresponding author. e-mail: h.a.dijkstra@uu.nl

Citation: Tellus A: 2017, **69**, 1299283, http://dx.doi.org/10.1080/16000870.2017.1299283

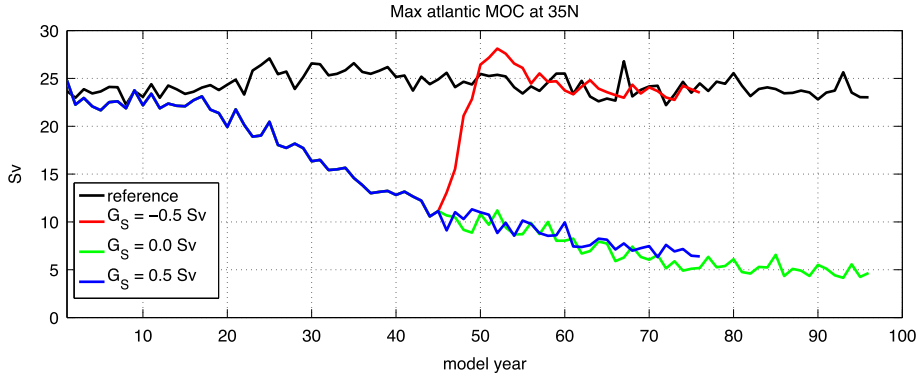

Fig. 1. Maximum AMOC at 35°N; the values of G_S are shown in the labeling of the curves. The black curve is the AMOC strength of the reference simulation.

Den Toom et al. (2014) analyzed results of a low-resolution and a high-resolution POP simulation having an integrated flux of freshwater near Greenland equal to 0.5 Sv. Based on a detailed study of the salt balance in the models, they found that the transient net freshwater advection by the overturning at the southern boundary of the Atlantic (Huisman et al., 2010), which forms a measure of the salt advection feedback, has an opposite sign in the low- and high-resolution versions of the model.

As suggested by Wolfe and Cessi (2009, 2011), water mass transformation theory (Marsh et al., 2000) can be used to relate the steady-state strength of the adiabatic, interhemispheric ('pole-to-pole') overturning circulation to the surface density distribution. This is achieved by incorporating the idea that Southern Ocean Ekman transport can maintain a deep overturning circulation in the absence of diapycnal mixing (Toggweiler and Samuels, 1995). An adiabatic pole-to-pole circulation exists when the following two conditions are met: (1) westerlies are present over the Southern Ocean, which drive a thermally indirect meridional flow and establish a deep stratification; and (2) there is a set of outcropping isopycnals that are shared between the Southern Ocean and the northern North Atlantic, providing a deep, adiabatic pathway for the southward return flow of North Atlantic Deep Water (NADW). The theory was extended (Nikurashin and Vallis, 2011) by including a diabatic abyssal overturning cell, corresponding to AntArctic Bottom Water (AABW).

In this study, the nonlinear behaviour of the AMOC and the associated water mass transformations in the North Atlantic due to freshwater perturbations around Greenland are investigated using the same strongly eddying global ocean model as in Weijer et al. (2012). We specifically consider the difference between the response of a strong AMOC to positive freshwater anomalies near Greenland and that of a weak AMOC to negative freshwater anomalies. Huge freshwater anomalies (0.5 Sv) are used to obtain a good signal-to-noise ratio to isolate the difference in the time scale of weakening/strengthening of the AMOC. An explanation for this asymmetry in AMOC response is proposed using water mass transformation theory.

2. Ocean model and simulations

The simulations described here are performed using the global version of the POP (Dukowicz and Smith, 1994; Maltrud et al., 2010), having a tripolar grid layout, with poles in Canada and Russia. The strongly eddying configuration has a nominal horizontal resolution of 0.1° and is the same as that used by Weijer et al. (2012). The vertical grid consists of 42 non-equidistant z-levels, increasing in thickness from 10 m just below the upper boundary to 250 m just above the lower boundary at 6000 m depth. The bottom topography is discretized using partial bottom cells, creating a more accurate and smoother representation of topographic slopes.

The atmospheric state is based on the repeat annual cycle (normal-year) Coordinated Ocean Reference Experiment (CORE[1]) forcing dataset (Large and Yeager, 2004), with the 6-hourly forcing averaged to monthly. Wind stress is calculated offline using the Hurrell Sea Surface Temperature (SST) climatology (Hurrell et al., 2008) and standard bulk formulae. Evaporation and sensible heat flux are calculated online using bulk formulae and the model predicted SST. Precipitation is also taken from the CORE forcing dataset. Ice cover is prescribed based on the $-1.8\,^{\circ}C$ isoline of the SST climatology, with both temperature and salinity restored on a timescale of 30 days under diagnosed climatological ice. This leads to artificial freshwater and heat fluxes that are at least an order of magnitude smaller than the mean fluxes and are only located within the region of the sea-ice.

The numerical simulations branch off from the end of year 75 of a spin up from rest under salinity restoring (Maltrud et al., 2010). The dependence of the salt flux on sea surface salinity is removed in the simulations described here. This is done by diagnosing the salt flux implied by the restoring condition from

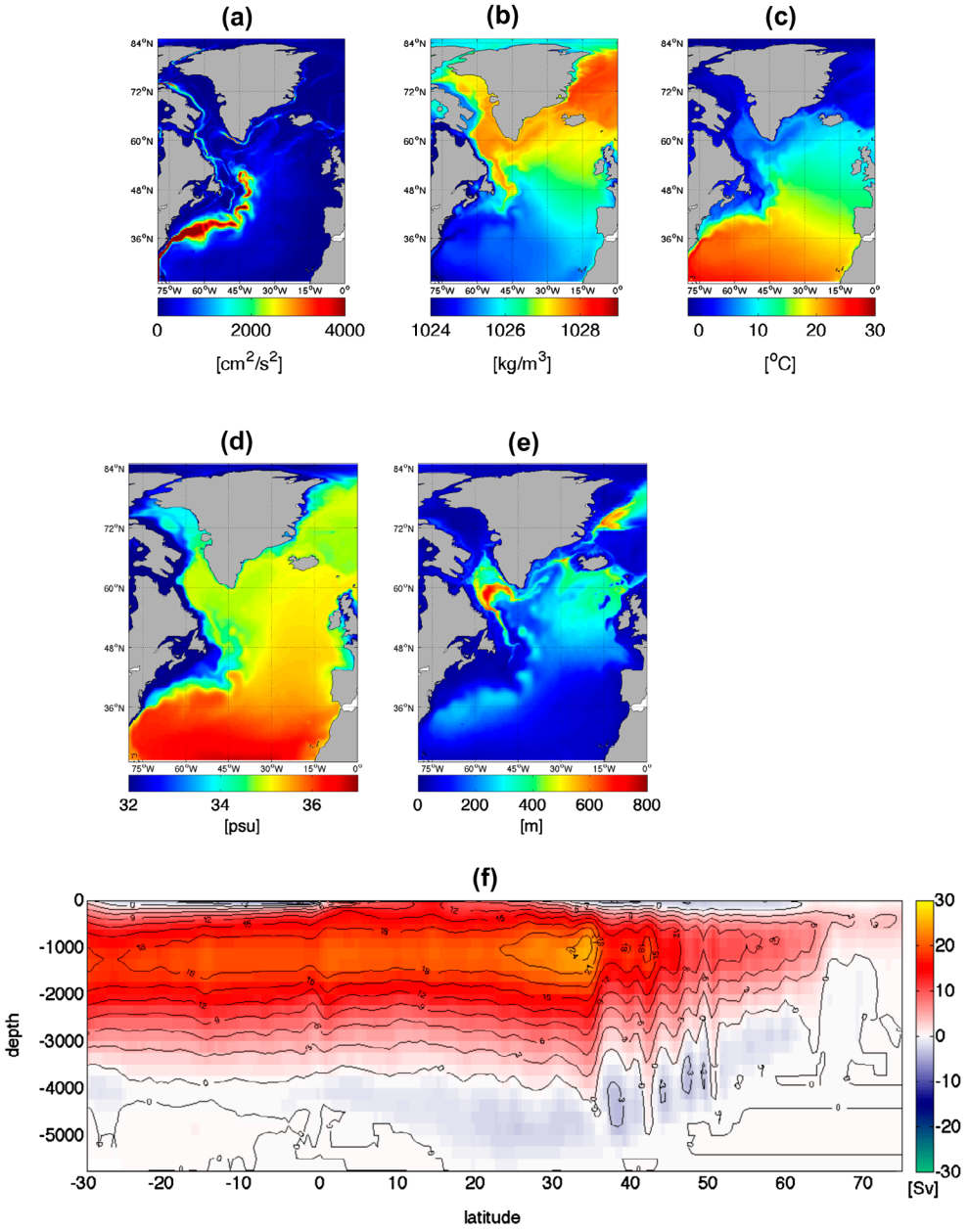

Fig. 2. Mean of model years 1–96 for the reference simulation: (a) kinetic energy (mean over the upper 50 m), (b) potential density (average over the upper 50 m), (c) temperature (mean over the upper 50 m), (d) salinity (mean over the upper 50 m), (e) maximum mixed layer depth in March, and (f) pattern of the AMOC.

the next 5 years (years 76–80) of the spin-up simulation and adding the result to the climatological fluxes. The annual mean field of the total freshwater flux is shown in Fig. 1a of Den Toom et al. (2014) and shows a good agreement with observations (e.g. the HOAPS dataset as in Fig. 16 of Andersson et al., 2010). Just to give an impression on the computational effort to perform simulations with this model: on 1296 cores of the Cartesius machine https://userinfo.surfsara.nl/systems/cartesius/description, the performance is about 4 model years per 24 h (van Werkhoven et al., 2014).

Apart from a control simulation, where no freshwater anomalies have been prescribed, three simulations have been performed. In the $G_S = 0.5$ Sv simulation, an additional 0.5 Sv of freshwater has been introduced around Greenland over 75 model years. The

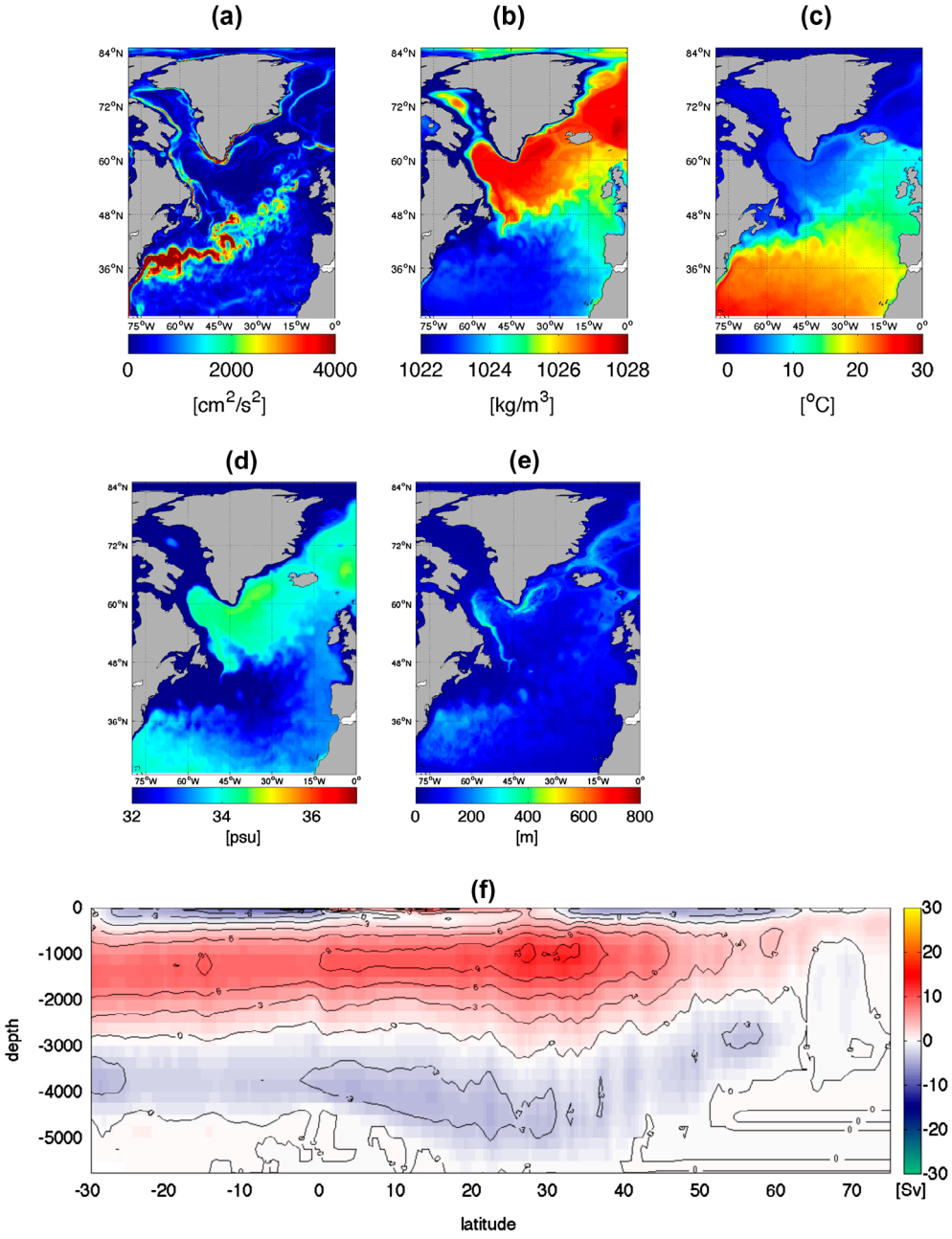

Fig. 3. Mean of model year 45 for the $G_S = 0.5$ simulation: (a) kinetic energy (mean over the upper 50 m), (b) potential density (average over the upper 50 m), (c) temperature (mean over the upper 50 m), (d) salinity (mean over the upper 50 m), (e) maximum mixed layer depth in March, and (f) pattern of the AMOC.

first 45 year of this simulation was analysed in Weijer et al. (2012) and Den Toom et al. (2014). After 45 model years, the second simulation ($G_S = 0.0$ Sv) branches off from the first simulation, only with the difference that the additional freshwater has been stopped; it runs for another 50 model years. The third simulation also starts from year 45 of the $G_S = 0.5$ Sv experiment but, instead of stopping the freshwater inflow, it is reversed resulting in a salt inflow (hence it is referred to as the $G_S = -0.5$ Sv simulation). The freshwater perturbation amplitudes are much larger than any realistic freshwater forcing which could result from present-day Greenland Ice Sheet melting (Böning et al., 2016). However, these amplitudes are used

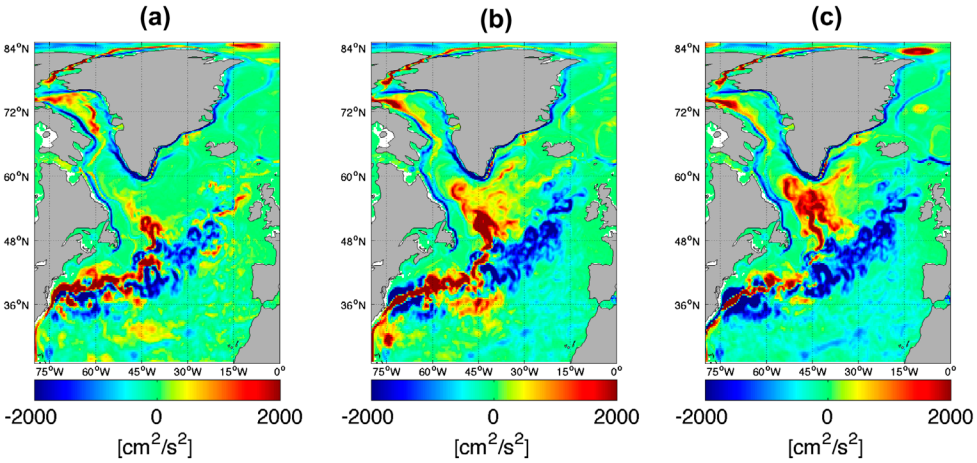

Fig. 4. Annual mean, upper 50 m averaged, kinetic energy difference of the $G_S = -0.5$ simulation w.r.t. mean of model year 45 of the $G_S = 0.5$ simulation; model year (a) 48, (b) 56, and (c) 76.

here to clearly identify the mechanism of the AMOC response asymmetry in strongly eddying models with strong internal variability (Den Toom et al., 2014).

3. Results

The presentation of the results is divided over two sections. In Section 3.1, we describe changes in the AMOC and associated fields such as the mixed layer depth, eddy kinetic energy and potential density. Section 3.2 provides a further analysis of the AMOC behavior in the different simulations using water mass transformation theory.

3.1. Response to freshwater anomalies

The maximum annual mean AMOC at 35°N slowly varies around 25 Sv in the reference simulation (black curve in Fig. 1). Although this maximum is also strongly coupled to the Gulf Stream transport, it adequately monitors the AMOC strength as the AMOC pattern is basin wide coherent (Buckley and Marshall, 2016). There is hardly any drift, which shows that the constructed freshwater flux from the spin-up simulation is able to maintain a statistical steady state. Under the freshwater forcing with $G_S = 0.5$ Sv, the AMOC decreases to about 10 Sv over the first 45 years and to about 7 Sv over the next 30 years (blue curve in Fig. 1). When terminating this freshwater perturbation after 45 model years, the AMOC does not recover but continues to decrease during the following 50 years where it remains at a level of about 5 Sv ($G_S = 0.0$ Sv, green curve in Fig. 1). However, when the freshwater inflow is reversed ($G_S = -0.5$ Sv), the AMOC needs less than a decade to recover (red curve in Fig. 1). It slightly overshoots the reference simulation for a short period of time and thereafter quickly approaches the level of the reference simulation.

We first consider properties of the reference simulation by averaging over the years 1–96, focusing on northern part of the North Atlantic (30°N– 85°N). The total kinetic energy (averaged over the upper 50 m) shown in Fig. 2(a) indicates strong boundary currents south of Greenland and in the Labrador Sea. It also shows a realistic Gulf Stream separation near Cape Hatteras and a turning of its continuation further downstream. Patterns of the potential density, temperature, salinity and maximum mixed layer depth (in March) are shown in Fig. 2(b)–(e). These are compatible with a strong AMOC which transports salt and heat northwards, creating a high density region in the Labrador Sea, with substantial convection (and associated deep winter mixed layers). The pattern of the AMOC, as shown in Fig. 2(f) shows that its maximum value is located at about 35°N and at 1000 m depth.

The freshwater input ($G_S = 0.5$ Sv) has a strong impact on the three-dimensional ocean circulation (Brunnabend et al., 2014). The Gulf Stream and North Atlantic current shift to the east (Fig. 3(a)) and transport less heat to the subpolar gyre region (Fig. 3(c)). In particular, the turning of the Gulf Stream continuation into the direction of Labrador Sea weakens, leading to a decreased upper ocean temperature in this region. However, the cooling cannot fully compensate for the decreased potential density caused by the freshening (Fig. 3(d)). In the regions of the North Atlantic deep water formation in the Labrador and Norwegian Sea, the potential density of the upper ocean is strongly decreased (Fig. 3(b)). As a consequence the maximum mixed layer depth is reduced substantially (Fig. 3(e)). In addition, the NADW return depth is shallowing by about 1500 m during the first 45 model years of the ($G_S = 0.5$ Sv) simulation giving the strengthened AABW cell the opportunity to fill the space (Fig. 3(f)).

When reversing the freshwater inflow at year 45 of the $G_S = 0.5$ Sv simulation, the AMOC recovers within 10 years (Fig. 1).

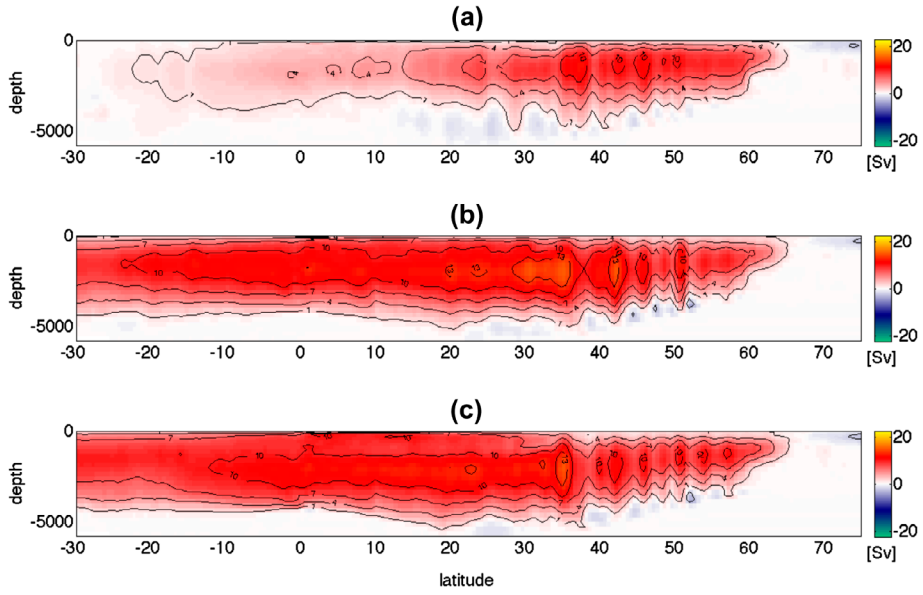

Fig. 5. Annual mean AMOC difference of the $G_S = -0.5$ simulation w.r.t. the mean of model year 45 of the $G_S = 0.5$ simulation; model year (a) 48, (b) 56, and (c) 76.

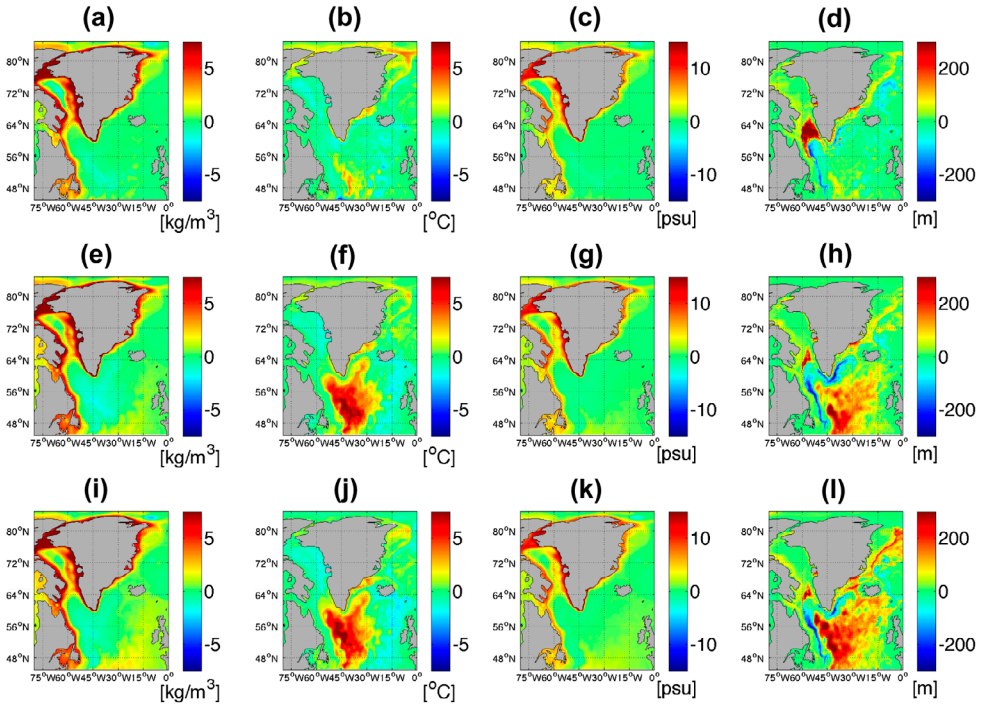

Fig. 6. Difference fields of the $G_S = -0.5$ simulation w.r.t. the mean of model year 45 of the $G_S = 0.5$ simulation. (a), (e), and (i) potential density (average over the upper 50 m), (b), (f), and (j) temperature (mean over the upper 50 m), (c), (g), and (k) salinity (mean over the upper 50 m), and (d), (h), and (l) maximum mixed layer depth in March; model year (a)–(d) 48, (e)–(h) 56, and (i)–(l) 76.

The differences of the annual mean kinetic energy patterns (with respect to that at year 45) for this $G_S = -0.5$ Sv simulation are shown for the years 48, 56 and 76 in Fig. 4. Within 10 years, the Gulf Stream separation has restored from an overshoot near Cape Hatteras (Fig. 4(a)) to a well separated current (Fig. 4(b)), while simultaneously its continuation is turning back into the Labrador

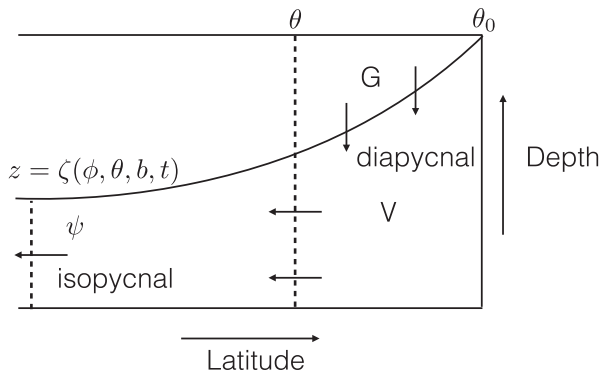

Fig. 7. Sketch of an isopycal which surfaces at $\theta = \theta_0$ and the associated diapycnal transport ψ (in Sv), isopycnal transport G (in Sv) and volume V changes (in m^3).

Sea (Fig. 4(c)). The width of the Gulf Stream is also decreasing, which clearly indicates a strong coupling between the buoyancy distribution in the northern North Atlantic, through the AMOC, to the Gulf Stream separation and width (Spall, 1996). It is also interesting that the boundary currents around the Labrador basin are generally weakening in strength during the recovery (Fig. 4(a)–(c)). Already 3 years after the salt anomaly has been applied, there is an 8 Sv increase in the AMOC through the North Atlantic (Fig. 5(a)). With time, this anomaly extends over the whole Atlantic basin and the return depth of the NADW increases (Fig. 5(b)). The maximum AMOC anomalies are largest in the Gulf Stream region (Fig. 5(c)).

The change in flow is immediately reflected in the differences (with respect to that at year 45) of temperature, salinity, potential density and maximum mixed layer depth fields in the northern North Atlantic (for the $G_S = -0.5$ Sv simulation) as shown for the years 48, 56, and 76 in Fig. 6. The signature of the applied salt perturbation can directly be seen in the salinity changes (Fig. 6(c), (g), and (k)), and this dominates also the potential density anomalies (Fig. 6(a), (e), and (i)) near the boundaries of Greenland and the Canadian coast. At year 48, the salt anomaly causes deep mixed layers only in the central Labrador Sea (Fig. 6(d)), but later such deep mixed layers are found over most of the area south of Greenland (Fig. 6(d), (h), and (l)). The recovery of the AMOC also leads to a strong northward heat transport, in particular through the changes in the surface circulation, that is shown as an increase in the temperature in the Labrador Sea (Fig. 6(b), (f), and (j)). The recovery of the AMOC also leads to a more than 5 °C temperature change south of Greenland.

3.2. *Analysis: water mass transformation theory*

The most remarkable result in the previous paragraph is the difference in time scales of collapse and restoring of the AMOC in the $G_S = 0.5$ Sv and $G_S = -0.5$ Sv simulations. We aim to explain this asymmetry in the AMOC response by using concepts from water mass transformation theory (Walin, 1982; Marsh et al., 2000) in the analysis of the model simulations. Consider in Fig. 7 an isopycnal, with constant density b, which surfaces at a latitude θ_0. In our results below, potential density referenced to 2000 m is used, that is $b = \sigma_2$. The vertical position of the isopycnal is given by $z = \zeta(\phi, \theta, b, t)$ as indicated in Fig. 7 and the volume below the isopycnal over the latitude range $[\theta, \theta_0]$ is V. The isopycnal overturning stream function is then defined as

$$\psi(\theta, b, t) = -r_0 \cos\theta \int_{\phi_W}^{\phi_E} \int_{-H}^{\zeta(\phi,\theta,b,t)} v(\phi, \theta, z, t)\, \mathrm{d}z\, \mathrm{d}\phi. \tag{1}$$

where H is the depth of the ocean bottom and r_0 is the radius of the Earth. Furthermore, ϕ_W and ϕ_E are the zonal boundaries of the domain and v the meridional velocity.

In transient situations, the isopycnal transport is not necessarily equal to diapycnal transport (Marsh et al., 2000). In addition to the isopycnal stream function ψ (in Sv), one therefore also needs to consider the change in time of V (in m^3), i.e.

$$V(\theta, b, t) = r_0^2 \int_{\theta}^{\theta_0} \cos\theta' \int_{\phi_W}^{\phi_E} \int_{-H}^{\zeta(\phi,\theta,b,t)} \mathrm{d}z\, \mathrm{d}\phi\, \mathrm{d}\theta', \tag{2}$$

which represents the volume north of the section at latitude θ and below the isopycnal with density b. A transformation 'pseudo' stream function

$$G(\theta, b, t) = \psi(\theta, b, t) + \frac{\partial V(\theta, b, t)}{\partial t}, \tag{3}$$

can then be defined, which has the useful property that its derivative with respect to latitude, $\partial G/\partial\theta$, gives the diapycnal flux at latitude θ. So, the two stream functions ψ and G are complementary; the first provides the isopycnal transport below the surface with buoyancy b, and the second monitors the diapycnal transport north of latitude θ (Marsh et al., 2000).

The fields of ψ, $\partial V/\partial t$ and G are shown for year 2 of the $G_S = 0.5$ simulation in Fig. 8(a), (e) and (i), respectively. The region of vertical contours near 60°N in Fig. 8(a) shows the sinking of water to deeper layers in the Labrador Sea. At this initial phase of the freshening, the isopycnals will move slightly downward. However, the deflation of the volume V, in particular for the deeper layers, is relatively weak (Fig. 8(e)). The sinking is here mainly associated with a diapycnal transformation (Fig. 8(i)). The difference between the three fields ψ, $\partial V/\partial t$ and G at year 46 and year 2 (Fig. 8(b), (f), and (j)) indicates that only in later stages of the development of the flow, the deflation of the deeper isopycnals becomes stronger, leading to a more negative $\partial V/\partial t$ at latitudes $\theta > 40$°N for $\sigma_2 \sim 37\,\mathrm{kgm}^{-3}$. Both the isopycnal and transformation stream function have substantially decreased as less water has access to the adiabatic pathway. This is due to the fact that less isopycnals are shared between the

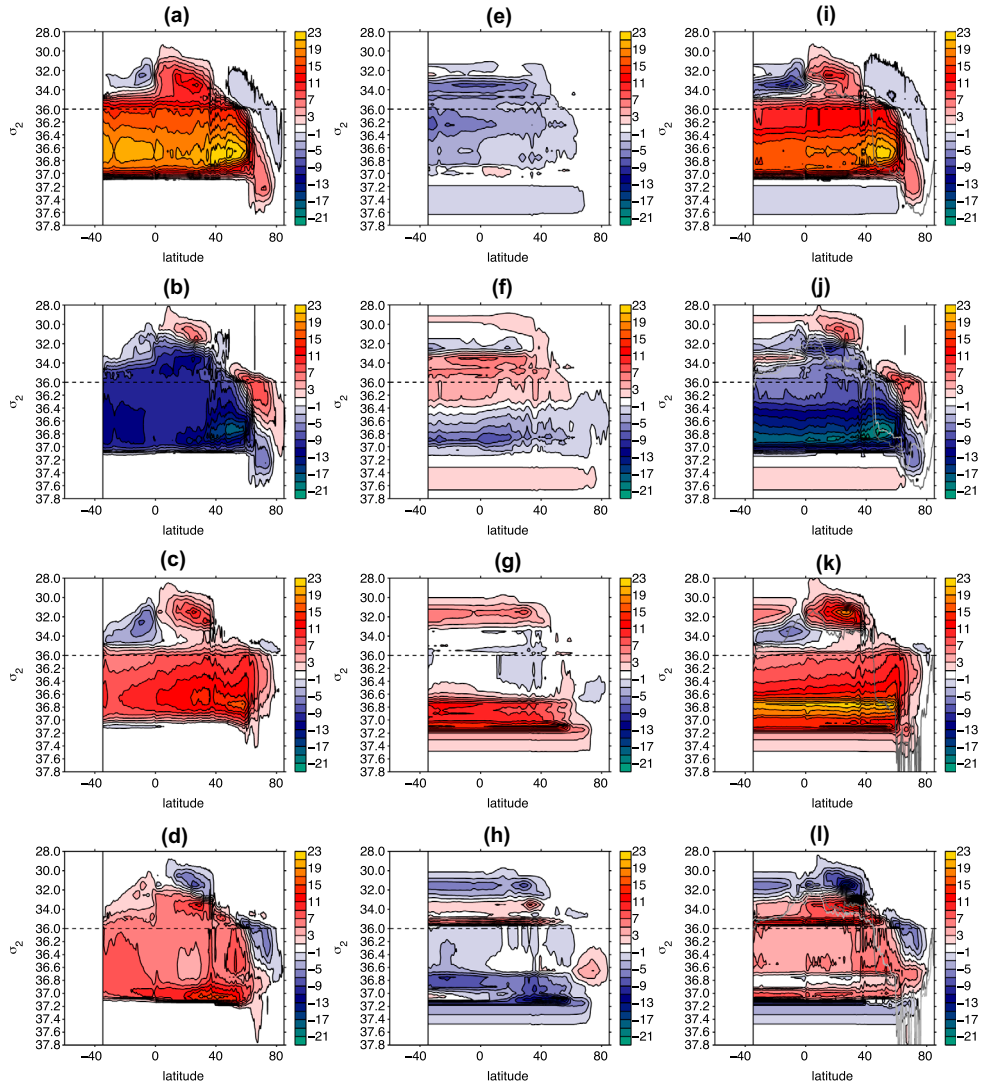

Fig. 8. (a)–(d) Isopycnal stream function ψ , (e)–(h) volume tendency $\partial V/\partial t$, and (i)–(l) transformation 'pseudo' stream function G of (a), (e), and (i) $G_S = 0.5$ Sv, model year 2, (b), (f), and (j) $G_S = 0.5$ Sv, model year 46 minus year 2, (c), (g), and (k) $G_S = -0.5$ Sv, model year 47, (d), (h), and (l) $G_S = -0.5$ Sv, model year 77 minus year 47.

northern North Atlantic and Southern Ocean (Wolfe and Cessi, 2009; Den Toom et al., 2014).

Two years after the salt input has started, the isopycnal stream function already is increasing in strength (Fig. 8(c)). The crucial difference with the behavior of the AMOC when freshwater is added, is the relatively large values of $\partial V/\partial t$, in particular for the deeper layers (Fig. 8(g)). This indicates that as soon as salt is added, increased mixing occurs which leads quickly to a surfacing of the isopycnals, inflating the volume V of the deep isopycnals. Also due to the reconnection of isopycnals in the North Atlantic and in the Southern Ocean, the water gains access to the adiabatic pathway leading to a large diapycnal flux at northern latitudes (Fig. 8(k)). At year 77, when the AMOC has already equilibrated to that of the reference simulation, the isopycnal stream function is only increased (compared to year 47) at depth (Fig. 8(d)). The inflation has nearly ceased at depth in the northern North Atlantic (Fig. 8(h)) and there is again a large diapycnal flux at deeper layers (associated with a full strength AMOC).

4. Summary and discussion

The response of the AMOC to freshwater perturbations continues to be a central theme in climate research. There is a wide diversity of AMOC responses to future increases of greenhouse gases in the CMIP5 climate models (IPCC, 2013) which is not very well understood. In this paper, we have focussed on a specific aspect: the difference between the response of a strong AMOC

to positive freshwater perturbations and of a weak AMOC to negative freshwater perturbations, where the perturbations were localized in the northern North Atlantic (i.e. near Greenland).

The main new element is that the simulations are done with a strongly eddying global ocean model. In this model, boundary currents such as the Gulf Stream and in the Labrador Sea are well represented and the flow is highly variable due to the presence of ocean eddies. Hence, the connection between changes in these boundary currents, deepening of the maximum mixed layer and the AMOC can be studied in more detail than in low-resolution models (e.g. Stammer et al., 2011) where the boundary currents are diffuse and the effects of eddies are parameterized.

Our main result is that the strong AMOC decays over about 50 years due to the freshwater perturbation, whereas the weak AMOC recovers in about 10 years due to the salt perturbation. Hence, there is about a factor of 5 difference between the time scale of the AMOC decrease and the AMOC increase. The main mechanism of the different response time scales can be understood from an analysis using water mass transformation theory. When the upper layer density decreases due to the freshwater input, the isopycnals move to lower depths. The motion of the isopycnals is controlled by advection and hence is relatively slow. As a consequence, there is a deflation in volume below an isopycnal ($\mathrm{d}V/\mathrm{d}t < 0$) and because also the diapycnal flux decreases, the isopycnal transport decreases. On the contrary, when salt water is added to a weak AMOC this leads to a rapid increase in the surface density through mixing and hence the isopycnal moves upward. This gives a rapid inflation in volume ($\mathrm{d}V/\mathrm{d}t > 0$) and because also the diapycnal transport increases, the isopycnal transport increases.

We used unrealistically large freshwater anomalies to obtain a high signal-to-noise-ratio of the response in this highly variable ocean model (Weijer et al., 2012), but there is a priori no reason why the mechanism of the asymmetric response would not be applicable under smaller freshwater forcing amplitudes. Hence, one would expect a weaker AMOC to respond quicker to negative freshwater anomalies on a decadal time scale than a stronger AMOC to positive freshwater anomalies. Unfortunately, nor the observational nor the high-resolution model data are available (Buckley and Marshall, 2016) to test whether one can detect such response asymmetries but it certainly is an interesting aspect to consider as it may be relevant for the response of the AMOC due to climate change.

Although not further analysed in this paper, there appears to be a strong coupling between the changes in density in the northern North Atlantic, the strength of the boundary currents and the strength of the AMOC. Changes in density affects convection, the strength of the boundary currents in the Nordic Seas and hence the deep water formation and path of the southward branch of the AMOC (Spall and Pickart, 2001). This in turn also influences the path of the Gulf Stream which overshoots to the north under a weakened deep return branch. To understand the full connection between the changes in the boundary currents and the AMOC changes, one has to combine the theories of deep sinking (Spall and Pickart, 2001), AMOC strength (Wolfe and Cessi, 2009) and of the interaction of deep and shallow boundary currents (Spall, 1996). The simulations of which results were presented here are less suitable to help develop such a theory as they consider quite a transient response and one rather would have equilibrium responses. The required equilibrium simulations for global strongly eddying ocean models are, however, not yet practical as they require at least 1000 model simulation years (and each would take us about a year to complete).

Acknowledgements

We thank Michael Kliphuis for carrying out the simulations of this study and for making the data available for analysis.

Disclosure statement

No potential conflict of interest was reported by the authors.

Funding

This work was supported by the Netherlands eScience Center (NLeSC) via the project eSALSA (An eScience Approach to determine future Sea-level chAnges) sponsored by the Netherlands Organization for Scientific Research (NWO). The simulations have been performed on the Cartesius supercomputer at SURFsara (https://www.surfsara.nl) through the [grant number SH 244-13], [grant number SH-244-15].

Note

1. see http://www.clivar.org/organization/wgomd/core/core.php

References

Andersson, A., Fennig, K., Klepp, C., Bakan, S., Graßl, H. and co-authors. 2010. The Hamburg Ocean atmosphere parameters and fluxes from satellite data – HOAPS-3. *Earth Syst. Sci. Data Discuss.* **3**(1), 143–194.

Behrens, E., Biastoch, A. and Böning, C. W. 2013. Spurious AMOC trends in global ocean sea-ice models related to subarctic freshwater forcing. *Ocean Model.* **69**(C), 39–49.

Böning, C. W., Behrens, E., Biastoch, A., Getzlaff, K. and Bamber, J. L. 2016. Emerging impact of Greenland meltwater on deepwater formation in the North Atlantic Ocean. *Nature Geosci.* **9**(7), 523–527.

Brunnabend, S.-E., Dijkstra, H. A., Kliphuis, M. A., van Werkhoven, B., Bal, H. E. and co-authors. 2014. Changes in extreme regional sea surface height due to an abrupt weakening of the Atlantic meridional overturning circulation. *Ocean Sci.* **10**, 881–891. DOI: 10.5194/os-10-881-2014.

Buckley, M. W. and Marshall, J. 2016. Observations, inferences, and mechanisms of the Atlantic meridional overturning circulation: A review. *Rev. Geophys.* **54**(1), 5–63.

Den Toom, M., Dijkstra, H. A., Weijer, W., Hecht, M. W. and Maltrud, M. E. 2014. Sensitivity of a strongly eddying global ocean to North Atlantic Freshwater Perturbations. *J. Phys. Oceanogr.* **44**, 464–481.

Drijfhout, S., Bathiany, S., Beaulieu, C., Brovkin, V., Claussen, M. and co-authors. 2015. Catalogue of abrupt shifts in intergovernmental panel on climate change climate models. *Proc. Natl. Acad. Sci.* **112**(43), E5777–E5786.

Dukowicz, J. K. and Smith, R. D. 1994. Implicit free-surface method for the Bryan–Cox–Semtner ocean model. *J. Geophys. Res.* **99**(C4), 7991–8014.

Gerdes, R., Hurlin, W. and Griffies, S. M. 2006. Sensitivity of a global ocean model to increased run-off from Greenland. *Ocean Model.* **12**, DOI: 10.1016/j.ocemod.2005.08.003.

Huisman, S. E., den Toom, M., Dijkstra, H. A. and Drijfhout, S. 2010. An indicator of the multiple equilibria regime of the Atlantic meridional overturning circulation. *J. Phys. Oceanogr.* **40**(3), 551–567.

Hurrell, J. W., Hack, J. J., Shea, D., Caron, J. M. and Rosinski, J. 2008. A new sea surface temperature and sea ice boundary dataset for the community atmosphere model. *J. Clim.* **21**(19), 5145–5153.

IPCC, 2013. Climate change 2013: The Physical Science Basis. In: Contribution of Working Group I to the Fifth Assessment Report of the Intergovernmental Panel on Climate Change (IPCC) (ed. T. F. Stocker, et al. Cambridge University Press, Cambridge.

Johns, W. E., Baringer, M. O. and Beal, L. M. 2011. Continuous, array-based estimates of Atlantic Ocean heat transport at 26.5 N. *J. Clim.* **24**, 2429–2449.

Kopp, R. E., Mitrovica, J. X., Griffies, S. M., Yin, J., Hay, C. C. and co-authors. 2010. The impact of Greenland melt on local sea levels: A partially coupled analysis of dynamic and static equilibrium effects in idealized water-hosing experiments. *Clim. Change* **103**, 619–625. DOI: 10.1007/s10584-010-9935-1.

Large, W. G. and Yeager, S. 2004. *Diurnal to decadal global forcing for ocean and sea-ice models: The data sets and flux climatologies*. Technical Report, National Center for Atmospheric Research, Boulder, CO, USA.

Maltrud, M., Bryan, F. and Peacock, S. 2010. Boundary impulse response functions in a century-long eddying global ocean simulation. *Environ. Fluid Mech.* **10**(1–2), 275–295.

Marsh, R., Desbruyeres, D., Bamber, J. L., de Cuevas, B. A., Coward, A. C. and co-authors. 2010. Short-term impacts of enhanced Greenland freshwater fluxes in an eddy-permitting ocean model. *Ocean Sci.* **6**(3), 749–760.

Marsh, R., Nurser, A., Megann, A. and New, A. 2000. Water mass transformation in the Southern Ocean of a global isopycnal coordinate GCM. *J. Phys. Oceanogr.* **30**(5), 1013–1045.

Murray, R. J. 1996. Explicit generation of orthogonal grids for ocean models. *J. Comput. Phys.* **126**, 251–273.

Nikurashin, M. and Vallis, G. 2011. A theory of deep stratification and overturning circulation in the ocean. *J. Phys. Oceanogr.* **41**(3), 485–502.

Spall, M. 1996. Dynamics of the gulf stream-deep western boundary current crossover. Part I: Entrainment and recirculation. *J. Phys. Oceanogr.* **26**, 2152–2168.

Spall, M. and Pickart, R. S. 2001. Where does dense water sink? A subpolar gyre example. *J. Phys. Oceanogr.* **31**, 810–826.

Stammer, D. 2008. Response of the global ocean to Greenland and Antarctic ice melting. *J. Geophys. Res.* **113**. C06022. DOI: 10.1029/2006JC004079.

Stammer, D., Agarwal, N., Herrmann, P., Köhl, A. and Mechoso, C. R. 2011. Response of a coupled ocean-atmosphere model to Greenland ice melting. *Surv. Geophys.* **32**, 621–642. DOI: 10.1007/s10712-011-9142-2.

Stommel, H. 1961. Thermohaline convection with two stable regimes of flow. *Tellus* **13**, 244–230.

Toggweiler, J. R. and Samuels, B. 1995. Effect of Drake Passage on the global thermohaline circulation. *Deep-Sea Res.* **42**, 477–500.

van Werkhoven, B., Maassen, J., Kliphuis, M., Dijkstra, H., Brunnabend, S. and co-authors. 2014. A distributed computing approach to improve the performance of the parallel ocean program (v2. 1). *Geosci. Model Dev.* **7**(1), 267–281.

Walin, G. 1982. On the relation between sea-surface heat flow and thermal circulation in the ocean. *Tellus* **34**(2), 187–195.

Weijer, W., Maltrud, M. E., Hecht, M. W., Dijkstra, H. A. and Kliphuis, M. A. 2012. Response of the Atlantic Ocean circulation to Greenland Ice Sheet melting in a strongly-eddying ocean model. *Geophys. Res. Lett.* **39**(9), L09606-1–L09609-6.

Wolfe, C. L. and Cessi, P. 2009. Overturning circulation in an Eddy–Resolving model: The effect of the pole-to-pole temperature gradient. *J. Phys. Oceanogr.* **39**(1), 125–142.

Wolfe, C. L. and Cessi, P. 2011. The adiabatic pole-to-pole overturning circulation. *J. Phys. Oceanogr.* **41**(9), 1795–1810.

Wolfe, C. L. and Cessi, P. 2014. Salt feedback in the adiabatic overturning circulation. *J. Phys. Oceanogr.* **44**(4), 1175–1194.